EPJ Web of Conferences **318**, 01003 (2025) https://doi.org/10.1051/epjconf/202531801003
AAPM-III 2025

Turbulent convection simulation in a square cavity

Abdikerim Kurbanaliev*, *Makburat* Kalbekova, *Chinara* Alieva, *Ziiada* Murzakmatova, and *Myktarbek kyzy* Suyumkan

Osh State University, Osh, Kyrgyzstan

Abstract. The significance of this study pertains to the development of alternative energy sources, including solar panels, the optimization of thermal management in contemporary computer system microcomponents, safety protocols for nuclear reactors. The investigation addressed the numerical simulation of natural convection executed in a two-dimensional approximation. A comparative analysis of the mean temperature and vertical velocity component profiles derived from these simulations indicated that the OFv8 and OFv9 versions of OpenFOAM yielded congruent results, whereas the outputs from OFv7 deviated. It was observed that the SGG model in OFv7 provided velocity component profiles at mid-height that were more accurate compared to the LRR model. Conversely, for the OFv8 and OFv9 versions, the accuracy of the numerical results declined. It was demonstrated that for the SGG model, the accuracy of the velocity profile is enhanced when employing the bounded Gauss limitedLinear 1 scheme for discretizing the convective term of the equations for R and ε, as opposed to using the upwind scheme. OFv7, OFv8, and OFv9 versions of the OpenFOAM suite were found to underestimate the maximum kinetic energy and Reynolds stress near the cold, left cavity wall. The findings are applicable to mathematical modeling of heat and mass transfer processes.

1 Introduction

The investigation of natural convection in enclosed cavities holds significant importance due to its relevance in a variety of scientific and technical applications, including building ventilation, cooling of microelectronic components in computer systems, nuclear reactor safety, heat exchangers, and solar thermal receivers [1, 2]. The challenges frequently encountered in experimental studies aimed at determining convection parameters have prompted the development of diverse methodologies for addressing natural convection problems [3–5].

The substantial enhancement in computational power and the advancement of numerical algorithms, which utilize systems of partial differential equations that consider the dynamic and thermal properties of the flow under specified initial and boundary conditions, have rendered the mathematical modeling of such problems both technically feasible and economically viable [4, 5].

* Corresponding author: kurbanaliev@rambler.ru

Modern computational fluid dynamics (CFD) techniques now allow for the mathematical modeling of natural convection using systems of partial differential equations. These equations account for the dynamic and thermal properties of the flow under specified initial and boundary conditions. The increasing accessibility and affordability of high-performance computing resources have made such simulations both technically feasible and economically viable for researchers and engineers alike.

This study focuses on the mathematical modeling of turbulent natural convection within an air-filled cavity. Numerical simulations were conducted using the buoyantSimpleFoam solver from the OpenFOAM open-source package, installed on Ubuntu 18.04 LTS [6].

The significance of this work extends beyond academic interest, as it has direct implications for several critical areas. Insights from this study can inform the design and efficiency of solar panels and other renewable energy technologies. The findings can contribute to optimizing cooling strategies for modern computer systems, particularly in managing heat dissipation from microcomponents. Understanding convection patterns in enclosed spaces is crucial for developing and improving safety protocols in nuclear reactor design.

2 Formulation of the problem

This study investigates the computational modeling of stable natural convection in a three-dimensional enclosure with a square cross-section [1]. The cavity under examination measures 0.75 meters in both height and width, with a depth of 1.5 meters, as illustrated in Figure 1. A temperature gradient is established by maintaining the left vertical wall at 50°C and the right vertical wall at 10°C. This configuration results in a Rayleigh number of (Ra) of 1.5×10^9, calculated based on the cavity's width W.

Empirical data suggests that when measured at a distance from the front and rear walls, the mean temperature and velocity distributions display characteristics similar to a two-dimensional flow. Furthermore, these distributions demonstrate antisymmetric properties along the cavity's diagonal axis. Given these observations, the researchers have opted to employ a two-dimensional approximation for their numerical simulations in this investigation.

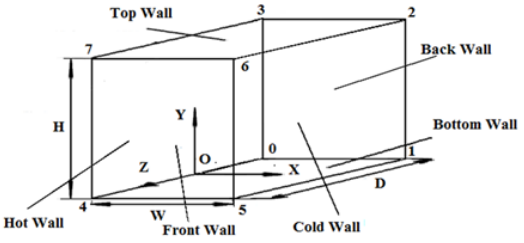

Fig. 1. Scheme of the cavity, vertex, computation domain boundaries and system of coordinate.

3 Mathematical model

The mathematical model of the problem under consideration is based on the system of Navier-Stokes equations [7]:

$$\nabla \cdot (\rho u) = 0, \tag{1}$$

$$\nabla \cdot (\rho u u) = -\nabla p + \rho g + \nabla \cdot \left(2\mu_{eff} D(u)\right) - \nabla\left(\frac{2}{3}\mu_{eff}(\nabla \cdot u)\right), \tag{2}$$

$$\nabla \cdot (\rho u h) + \nabla \cdot (\rho u k) = \nabla \cdot \left(\alpha_{eff} \nabla h\right) + \rho u \cdot g. \tag{3}$$

Here ρ is the density, p is the static pressure, g is the gravitational acceleration vector, μ_{eff} is the effective viscosity equal to the sum of the molecular and turbulent viscosities, h is the enthalpy, $k = 0.5|u|^2$ is the kinetic energy per unit mass, and $D(u)$ is the strain rate tensor is defined as

$$D(u) = 0.5(\nabla u + (\nabla u)^T)$$

Effective thermal diffusivity coefficient of α_{eff} is equal to the sum of the laminar and turbulent thermal diffusivity:

$$\alpha_{eff} = \frac{\rho \nu_t}{Pr_t} + \frac{\mu}{Pr} = \frac{\rho \nu_t}{Pr_t} + \frac{k}{C_p}$$

where k is the thermal conductivity coefficient, C_p is the specific heat at constant pressure, μ is the dynamic viscosity, ν_t is the turbulent kinematic viscosity, Pr is the Prandtl number, Pr_t is the turbulent Prandtl number.

In the OpenFOAM package, the terms in equation (2) associated with the static pressure gradient and the gravitational acceleration vector are written as follows:

$$-\nabla p + \rho g = -\nabla\left(p_{rgh} + \rho g \cdot r\right) + \rho g = -\nabla p_{rgh} - (g \cdot r)\nabla\rho - \rho g + \rho g = \\ = -\nabla p_{rgh} - (g \cdot r)\nabla\rho,$$

where $p_{rgh} = p - \rho g \cdot r$, and r is the radius vector.

The LRR [8] and SSG [9] turbulence models were used to simulate Reynolds stresses.

4 Numerical model

OpenFOAM blockMesh utility was used for creation of mesh. The control volume method is used for discretization of the transport equations (1-3) employs [10-12]. Table 1 presents the discretization schemes applied to each term of equations (1-3) related to the gradient, divergence, and Laplacian.

Table 1. Discretization schemes.

Scheme / Variable	gradSchemes	divSchemes	laplacianSchemes
Velocity, U	Gauss linear	bounded Gauss linearUpwind gradf(U)	Gauss linear corrected
Enthalpy, h	Gauss linear	bounded Gauss limitedLinear 1	Gauss linear corrected
Dissipation rate, ε	Gauss linear	bounded Gauss limitedLinear 1 Gauss upwind	Gauss linear corrected
Reynolds stress, R	Gauss linear	bounded Gauss limitedLinear 1 Gauss upwind	Gauss linear corrected

The more information about boundary conditions in this simulation one can find in Table 2.

Table 2. Used boundary conditions.

Boundary / Variable	Top Wall	Bottom Wall	Hot Wall	Cold Wall
Velocity, U	noSlip	noSlip	noSlip	noSlip
Temperature, T	fixedValue	fixedValue	50 °C	10 °C
Pressure, p_{rgh}	FixedFluxPressure	FixedFluxPressure	FixedFluxPressure	FixedFluxPressure

Dissipation rate, ε	epsilonWall Function	epsilonWall Function	epsilonWall Function	epsilonWall Function
Reynolds stresses, R	kqRWallFunction	kqRWallFunction	kqRWallFunction	kqRWallFunction

Since this study involves two-dimensional numerical simulation, appropriate boundary conditions were specified for four of the six boundaries of the computational domain: the top wall (Top Wall), bottom wall (Bottom Wall), hot wall (Hot Wall), and cold wall (Cold Wall). The remaining two boundaries, the front wall (Front Wall) and the back wall (Back Wall), are designated as empty in 2D simulations according to the OpenFOAM framework [6], and thus, do not require boundary conditions.

On the cavity walls, the no-slip condition was applied to the velocity vector. Boundary conditions for temperature on the upper and lower walls were derived from experimental data.

The pressure at all four boundaries was set to the fixedFluxPressure condition, which imposes a pressure gradient of 1.0×10^5 Pa, aligning the flow with the velocity boundary condition. Boundary conditions for the Reynolds stresses R and the turbulent kinetic energy dissipation rate of epsilon were specified using wall functions [10, 11].

The well-known algorithm SIMPLE [10-12] was employed to solve the pressure-related nonlinear equations, with the accuracy of the iterative process for the primary variables set to 1×10^{-4}. Under-relaxation coefficients were set as follows: 0.3 for velocity, 0.5 for enthalpy h, 0.2 for Reynolds stresses R, 0.7 for pressure p_{rgh}, and 0.5 for the kinetic energy dissipation rate ε.

Calculations were performed on three uniform grids: 200×200, 300×300, and 400×400, using different versions of the OpenFOAM package - OpenFOAM v7, OpenFOAM v8, and OpenFOAM v9. The bounded Gauss limitedLinear 1 and Gauss upwind discretization schemes were applied for the convective term discretization in the equations for Reynolds stresses R and the dissipation rate of kinetic energy ε (see Table 1).

5 Results of numerical calculations

Convergence graphs of the iterative process of the OpenFOAMv7 package for a 300×300 mesh are shown in Figures 2-3.

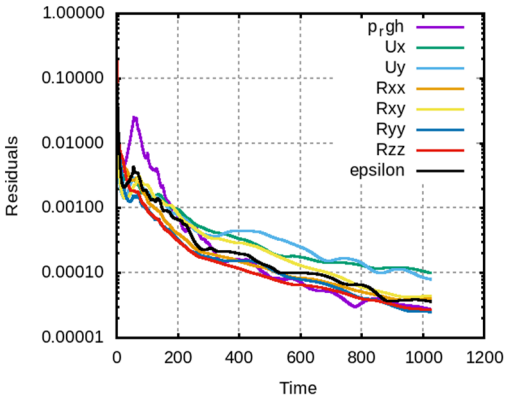

Fig. 2. Residuals for LRR model.

In the following Figures 4-21 the results of numerical calculations performed by different versions of the OpenFAOM package using LRR turbulence model with the corresponding

experimental data are compared [1]. The presented numerical data on the average temperature were obtained using the bounded Gauss limitedLinear 1 scheme to discretize the equations for R and ε.

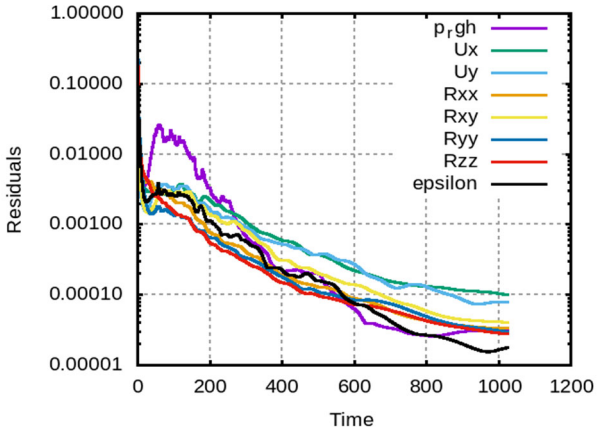

Fig. 3. Residuals for SSG model.

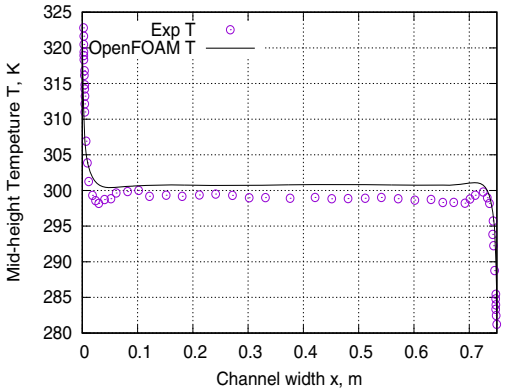

Fig. 4. Profile T on the mid-height when y=0.375 m, OFv7.

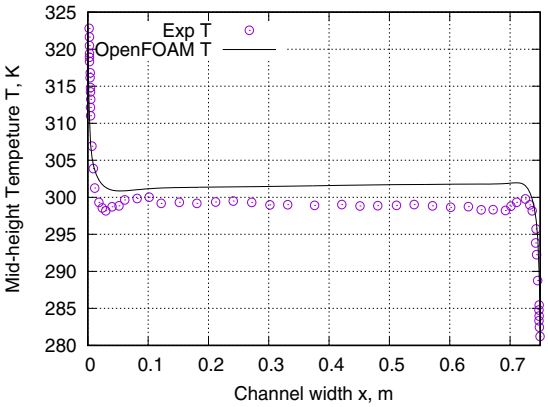

Fig. 5. Profile T on the mid-height when y=0.375 m, OFv8.

As can be seen from Figures 4-6, OpenFAOMv8 (see Figure 5) and OpenFAOMv9 (see Figure 6) almost give the same overestimated values of mean temperature, while the numerical data of OpenFAOMv7 (see Figure 4) are closer to the experiment.

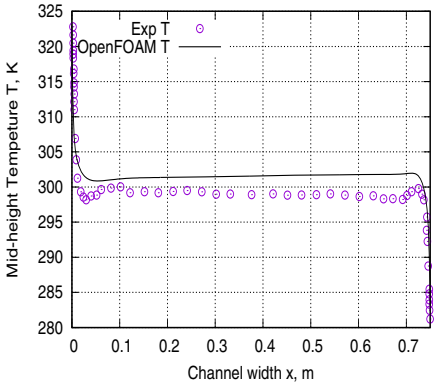

Fig. 6. Profile T on the mid-height when y=0.375 m, OFv9.

As it can be seen from Figures 7-9, the vertical velocity profiles Uy near the hot wall conform very well with the experiment for the three versions of OpenFAOM used. However, near the cold, right wall, OpenFAOMv7 gives slightly lower values, while the other two versions of OpenFAOM show the best results.

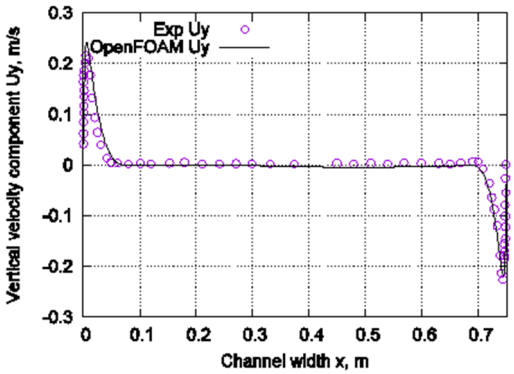

Fig. 7. Profile Uy on the mid-height when y=0.375 m, OFv7.

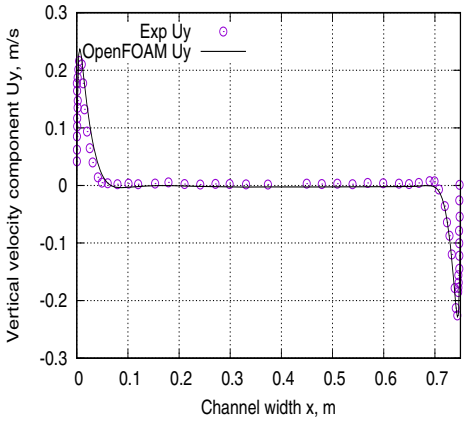

Fig. 8. Profile Uy on the mid-height when y=0.375 m, OFv8.

As observed in Figures 10-12 and Figures 13-15, the profiles of turbulent kinetic energy, defined as \(k = 0.5 \times (R_{xx} + R_{yy} + R_{zz}) \), and the Reynolds stress \(R_{xy} \), align with the corresponding experimental data. However, all three versions of the OpenFOAM package yield underestimated values for the maximum kinetic energy and Reynolds stress near the cold left wall of the cavity.

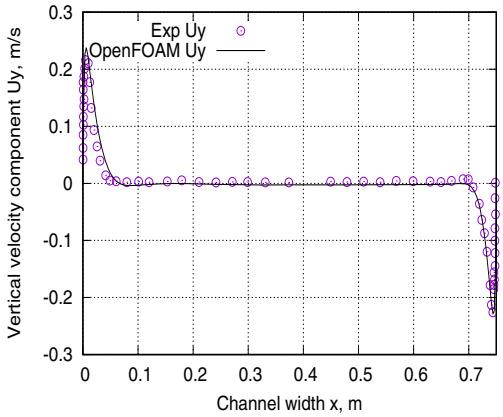

Fig. 9. Profile Uy on the mid-height when y=0.375 m, OFv9.

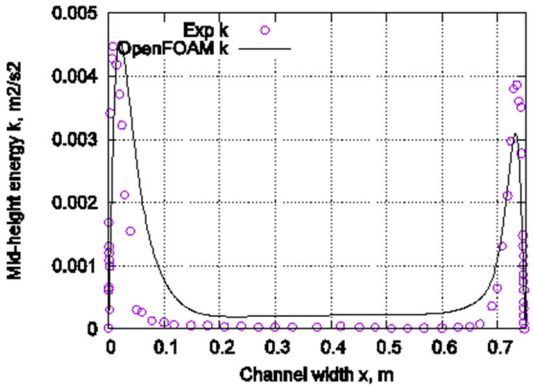

Fig. 10. Profile *k* on the mid-height when y=0.375 m, OFv7.

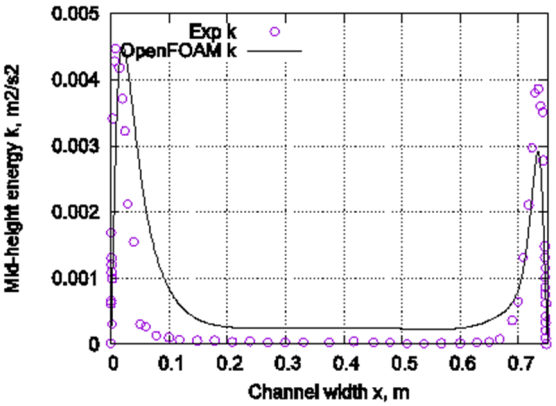

Fig. 11. Profile *k* on the mid-height when y=0.375 m, OFv8.

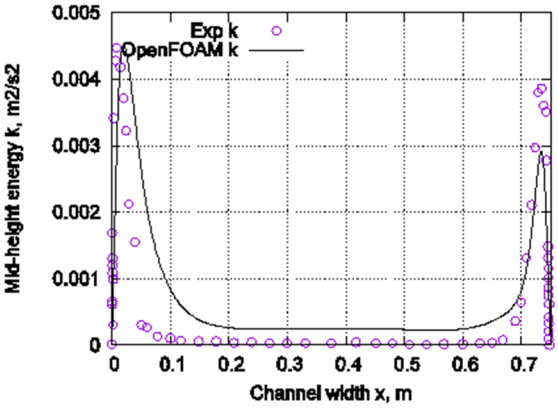

Fig. 12. Profile *k* on the mid-height when y=0.375 m, OFv9.

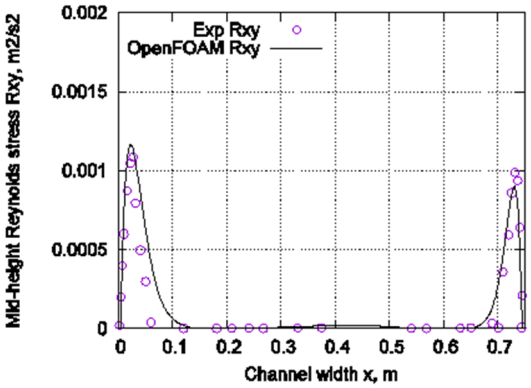

Fig. 13. Profile R_{xy} on the mid-height when y=0.375 m, OFv8.

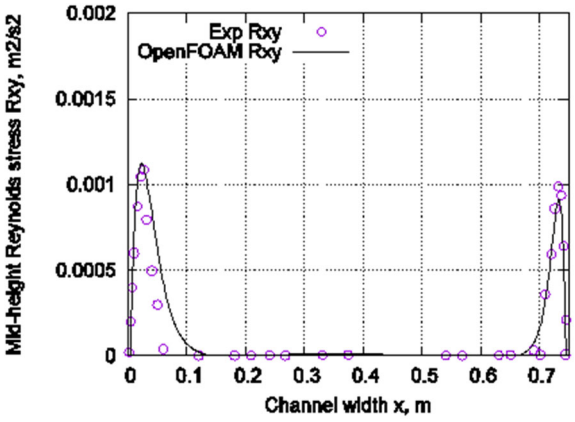

Fig. 14. Profile R_{xy} on the mid-height when y=0.375 m, OFv8.

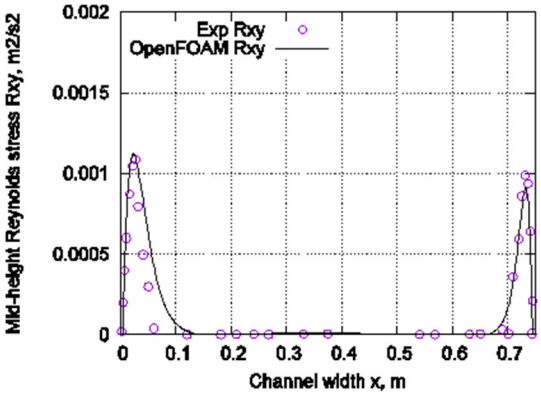

Fig. 15. Profile R_{xy} on the mid-height when y=0.375 m, OFv9.

If the three versions of the package for mean temperature profiles at the mid-width of the cavity give approximately the same values (see Figures 16-18), then there are differences in the results of predicting the field Ux of the velocity component at the average length of the cavity at x=0.375 m (see Figures 19-21).

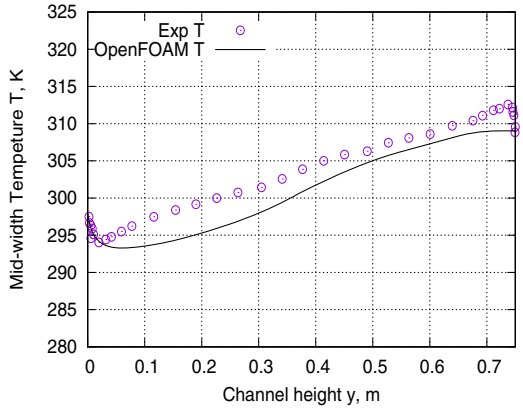

Fig. 16. Profile *T* on mid-width when x=0.375 m, OFv7.

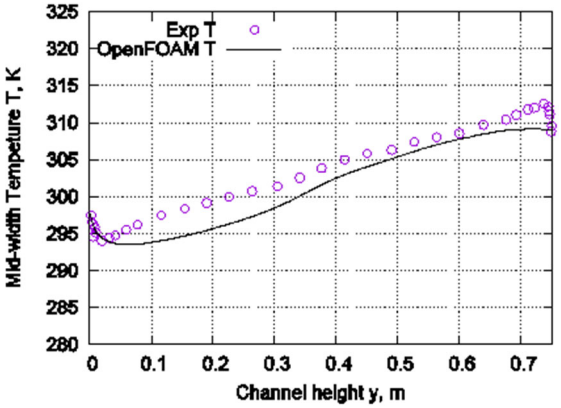

Fig. 17. Profile *T*on mid-width when x =0.375 m, OFv8.

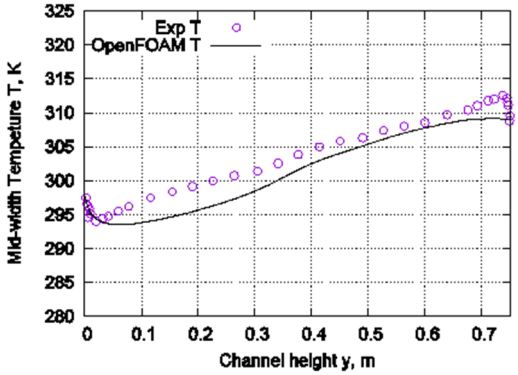

Fig. 18. Profile *T*on mid-width when x =0.375 m, OFv9.

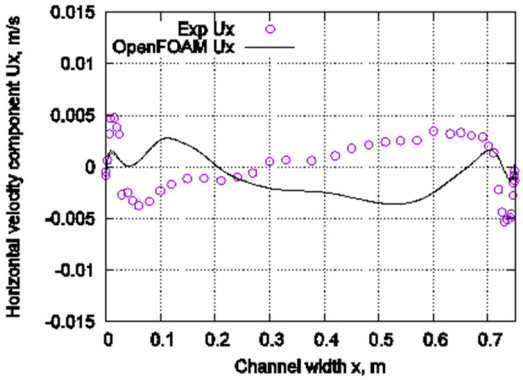

Fig. 19. Profile Ux on mid-height when y=0.375 m, OFv7.

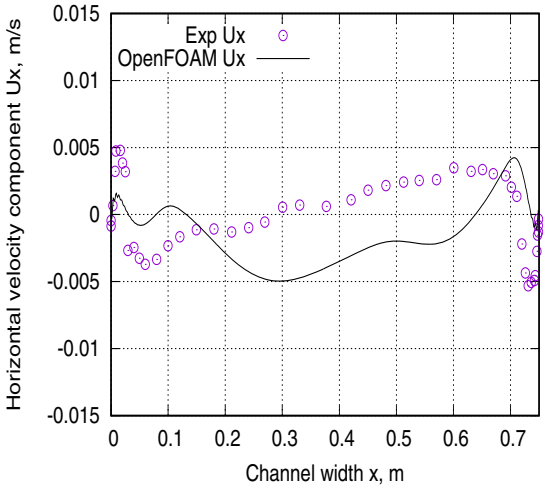

Fig. 20. Profile Ux on mid-height when y =0.375 m, OFv8.

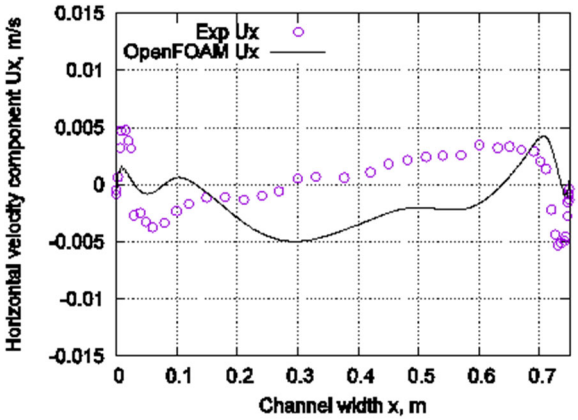

Fig. 21. Profile Ux on mid-height when y =0.375 m, OFv9.

The calculated and experimental velocity profiles Ux for the LRR and SGG turbulence models are shown in Figures 22-24 (LRR) and Figures 25-27 (SGG). The upwind scheme was used to discretize the convective term in the equations for R and ε.

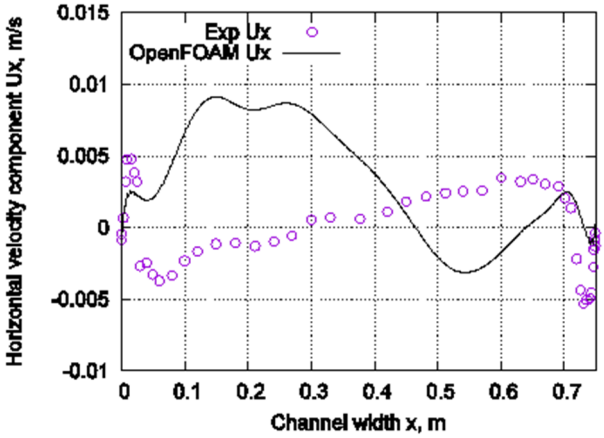

Fig. 22. Profile Ux on mid-height when y =0.375 m, OFv7.

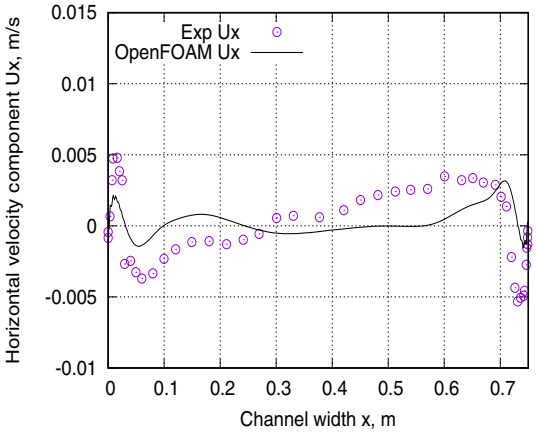

Fig. 23. Profile Ux on mid-height when y =0.375 m, OFv8.

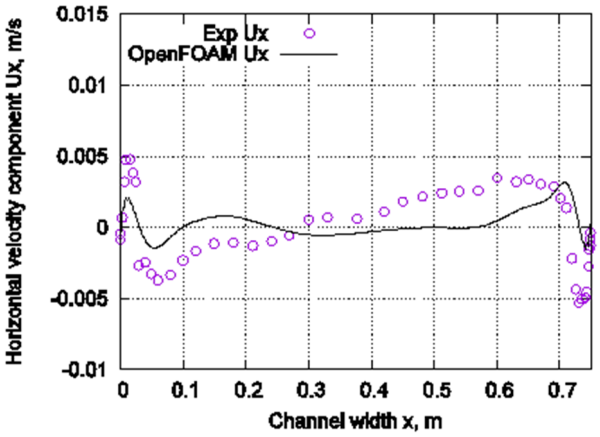

Fig. 24. Profile Ux on mid-height when y =0.375 m, OFv9.

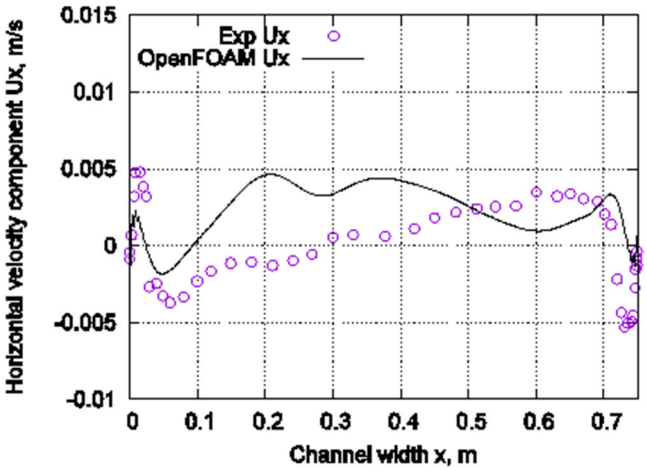

Fig. 25. Profile Ux on mid-height when y =0.375 m, OFv7.

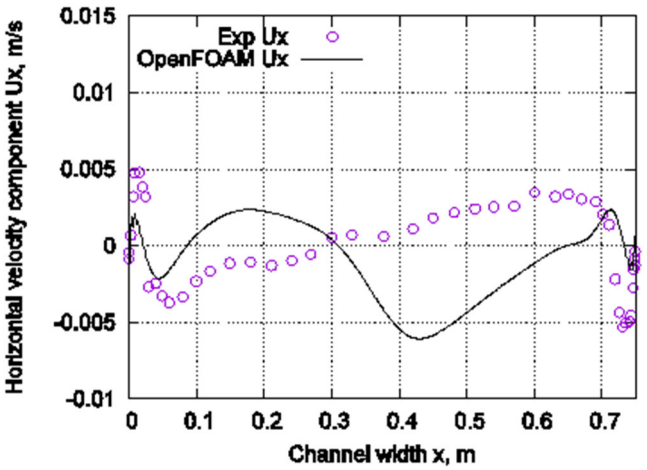

Fig. 26. Profile Ux on mid-height when y =0.375 m, OFv8.

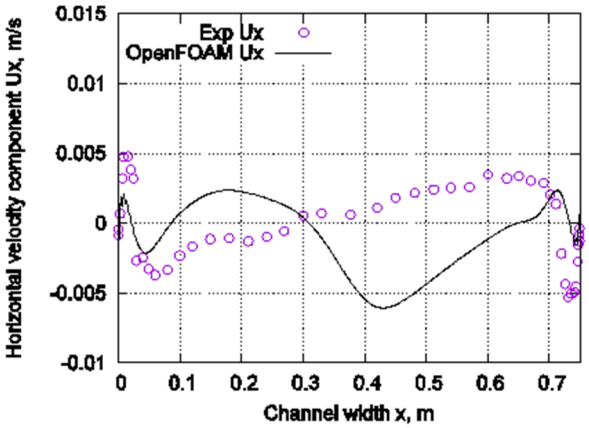

Fig. 27. Profile Ux on mid-height when y =0.375 m, OFv9.

As it can be seen from these figures, if for OFv7 SGG model gives closer values of the horizontal profile Ux of the velocity component at a mid-height at y = 0.375 m compared to LRR model, then for the OFv8 and OFv9 packages the situation is reversed – the accuracy of the numerical results deteriorates.

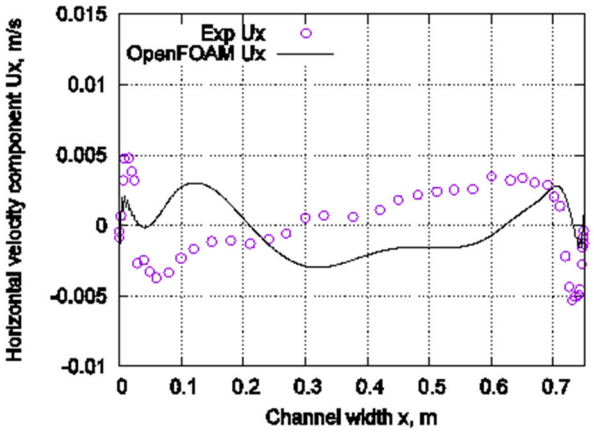

Fig. 28. Profile Ux on mid-height when y =0.375 m, OFv7.

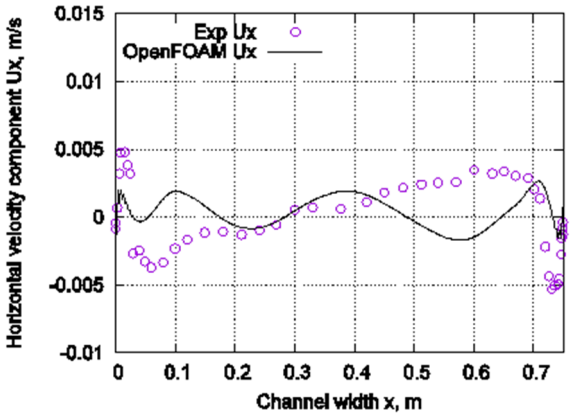

Fig. 29. Profile Ux on mid-height when y =0.375 m, OFv8.

For the SGG model, the accuracy of the numerical results of the velocity profile Ux when using the bounded Gauss limitedLinear 1 scheme to discretize the convective term of the equations for R and ε is higher (see Figures 25-27) than when using the upwind scheme (see Figures 28-30).

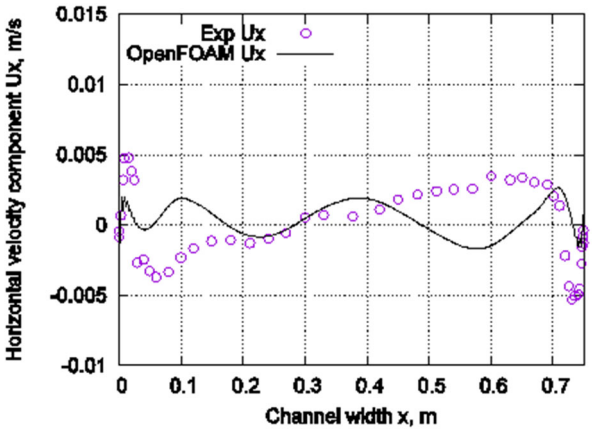

Fig. 30. Profile Ux on mid-height when y =0.375 m, OFv9.

In general, as evidenced by the previous figures, the OFv8 and OFv9 packages produce approximately the same results for all considered parameters of the convective flow, whereas the simulation results from the OFv7 package differ from those obtained with OFv8 and OFv9.

6 Conclusion

2D natural convection numeric modelling an air-filled square cavity was conducted. A comparison of the mean temperature and vertical velocity profiles from the simulations indicates that the OFv8 and OFv9 packages yield approximately identical results, while the results from OFv7 diverge from these. It was observed that for the OFv7 package, the SGG model provides velocity component Ux profiles at the average height y = 0.375 m that are closer to the experimental values compared to the LRR model. Conversely, for the OFv8 and OFv9 packages, the accuracy of the numerical results deteriorates with the SGG model.

Additionally, it was demonstrated that the accuracy of the velocity profile Ux using the SGG model is higher when employing the bounded Gauss limitedLinear 1 scheme for discretizing the convective term of the equations for R and ε compared to using the upwind scheme. Furthermore, it was found that all three versions of the OpenFOAM package, OFv7, OFv8, and OFv9, underestimate the maximum Reynolds stress and kinetic energy near the cold, left wall of the cavity.

References

1. F. Ampofo, T. Karayiannis, Turbulent natural convection in a square cavity, in *Proceedings of the 8th UK National Heat Transfer Conference* (Oxford, UK, 2003).
2. S.M. Aithal, Journal of Thermophysics and Heat Transfer **30(4)**, 843-853 (2016).
3. A. Baïri, J.M. García de María, I. Baïri, N. Laraqi, E. Zarco-Pernia, N. Alilat, International Journal of Heat and Mass Transfer **55(19-20)**, 4970-4980 (2012).

4. P. Abimanyu, A. Baïri, N. Nithyadevi, International Journal of Numerical Methods for Heat and Fluid Flow **26(8)**, 2528-2242 (2016).
5. V.I. Raschikov, A.S. Roshal, *Numerical Methods for Solving Physical Problems*, (Lan, St. Petersburg, Russia, 2005).
6. *Home of OpenFOAM, the CFD Software Licensed Free and Open Source Only*, https://openfoam.org/, last accessed 11.1.2024
7. *OpenFOAM7 User Guide*, https://cfd.direct/openfoam/user-guide-v7/, last accessed 11.1.2024
8. B.E. Launder, G.J. Reece, W. Rodi, Journal of Fluid Mechanics **68**, 537-566 (1975).
9. C.G. Speziale, S. Sarker, T.B. Gatski, Journal of Fluid Mechanics **227**, 245-272 (1991).
10. J.H. Ferziger, M. Peric, *Computational Methods for Fluid Dynamics*, (Springer Verlag, Berlin, Germany, 2002).
11. H.K. Versteeg, W. Malalasekera, *An Introduction to Computational Fluid Dynamics: The Finite Volume Method*, (Pearson Education Limited, Edinburg, UK, 2007).
12. S.V. Patankar, *Numerical Heat Transfers and Fluid Flow*, (Hemisphere Publishing Corporation, New York, UK, 1980).